Nanometer hypervelocity dust impacts in low Earth orbit

J. D. Carpenter,[1] T. J. Stevenson,[1] G. W. Fraser,[1] J. C. Bridges,[1] A. T. Kearsley,[2] R. J. Chater,[3] and S. V. Hainsworth[4]

[1] A study has been made of 60 nm thick aluminum films which have been exposed to the space environment outside of International Space Station (ISS) between 2002 and 2004. Field emission scanning electron microscopy has been used to provide high-resolution images of impact features less than 100 nm in diameter and of detailed impact morphologies at different spatial scales. Analysis of images reveals the incident directions and diameters of the impacting particles and allows separation of impacts at hypervelocity from those at lower velocities. This allows the separation of different particle populations. We find that most detected particles have been generated locally as the result of secondaries following larger impacts elsewhere on the ISS or as a result of docking maneuvers by the Progress supply module or by other spacecraft. There is also evidence for a population of dust particles incident at hypervelocity and with minimum diameters smaller than 10 nm. This particle flux of the dust particles is consistent with the expected flux of micrometeoroids with mass $>10^{-18}$ g at 1 AU and may represent the first measurement of dust particles with such small masses in near-Earth space. Future experiments to measure the flux of nanometer-scale dust particles are proposed, both passive exposure cells for retrieval and also active detectors to provide access to dust/debris populations without the requirement for experiment retrieval.

1. Introduction

[2] The solar system is pervaded by dust particles with masses less than 1 g and whose lifetimes have been shown to be much less than the age of the solar system [e.g., *Whipple*, 1967]. Any dust present in the solar system must therefore have a presently existing source. The majority of dust originates from comets and asteroids; interstellar dust has also been detected, passing through the solar system [*Grün et al.*, 2001]. After liberation from a parent body, a dust particle will be modified by the environments it encounters. The detection and analysis of dust particles therefore provides a means of probing the environments encountered by the particles and accessing their parent bodies.

[3] The flux of dust particles has been determined both by in situ measurements of dust impacts and by models [e.g., *Divine*, 1993]. The dust flux at 1 AU is typically obtained from the "Grün" interplanetary flux model [*Grün et al.*, 1985], which gives fluxes for particles with masses in the range 10^{-18} to 1 g. For particles with masses in the approximate range 10^{-15} to 10^{-5} g the Grün flux has been scaled to data from spacecraft at 1 AU. For particles as small as 10^{-18} the fluxes are determined from analyses of lunar microcraters. No flux data in the 10^{-18} g mass regime have been obtained from in situ spacecraft measurements, even though dust particle fluxes are dominated by the smallest particles. This is because, to date, no technique for dust impact detection has had sufficient sensitivity to access these particles.

[4] Dust particle impacts, used to determine particle fluxes, have been detected in space by a variety of techniques. The most simple dust flux experiments monitor the number of perforations or craters, generated by dust impacts, which appear in surfaces exposed to the space environment. Real-time detection of dust particles was originally performed by simple penetration detectors, while more recent instrumentation measures the ionization that occurs as a result of a dust impact. Instruments such as the Cosmic Dust Analyzer (CDA) on Cassini [*Srama and Grün*, 1997] and the proposed Large Area Mass Analyzer (LAMA) instrument [*Srama et al.*, 2007] are also able to obtain time of flight mass spectra, following this ionization, and thus derive the compositions of incident particles. A review of dust instrumentation and detection techniques is given by *Auer* [2001]. In all cases the sensitivity of instrumentation is a function of both particle mass and velocity. At a typical interplanetary

[1]Space Research Centre, Department of Physics and Astronomy, University of Leicester, Leicester, UK.
[2]Natural History Museum, London, UK.
[3]Department of Materials, Imperial College London, London, UK.
[4]Department of Engineering, University of Leicester, Leicester, UK.

dust velocity of 20 km s^{-1}, dust detectors flown to date have had a typical sensitivity to particles with masses greater than 10^{-15} g. The dust detector on HEOS 2 had a sensitivity to particle masses $>2 \times 10^{-16}$ g at 20 km s^{-1} [*Grün et al.*, 2001].

[5] Perforations and craters may be measured by either active impact detectors on spacecraft or, more commonly, by the analysis of surfaces retrieved from orbit and returned to Earth, where empirical hole and crater growth relationships can be used to infer particle parameters from impact hole and crater sizes [*McDonnell et al.*, 2001]. Surveyed surfaces and foils have primarily been those exposed on the Long Duration Exposure Facility (LDEF) [*McDonnell et al.*, 1993] and the solar cells retrieved from the Hubble Space Telescope during two servicing missions and from the retrieved European Retrievable Carrier (EURECA) spacecraft [*Drolshagen et al.*, 1996]. These data sets are limited to particles with diameters greater than approximately 100 nm and masses greater than approximately 10^{-15} g.

[6] Between 2002 and 2004 an experiment which was analogous to the simple passive penetration experiments exposed to space on previous missions was exposed to the external environment of the International Space Station before retrieval and return to Earth for analysis. For particle impacts at 20 km^{-1} the material exposed was sensitive to perforations by particles as small as 6.7×10^{-18} g. The detection technique could also provide a preliminary stage for an active and highly sensitive dust detection instrument.

[7] The experiment consisted of two microchannel plates (MCPs) with 12.5 μm diameter circular channels, bearing 60 nm thick evaporated aluminum films across their open areas (manufactured by Photonis SAS, Brive, France). The MCPs were exposed on the outside of the ISS's "Pirs" docking module as part of the Expose experiment to determine the effects of the ISS environment on X-ray optics [*Hofer*, 2004]. The standard "night vision" MCPs were thermally and mechanically representative of the square channel MCP X-ray optics intended for use on the Lobster X-ray telescope [*Fraser et al.*, 2001], whose intended platform was originally the European Space Agency's Columbus module on the ISS. Aluminum films on MCP optics act as low-absorbtivity thermal barriers to reduce stresses on the optics structure. The effects of contamination and erosion on the films during the exposure are described by *Carpenter et al.* [2006], and the results of early observations of submicron impact features on the films using secondary electron (SE) imaging with a scanning electron microscope (SEM) are reported by *Carpenter et al.* [2005]. The latter analysis of impacts revealed film perforations caused by a population of submicron dust particles and showed that the sensitivity of these very thin films to impacts exceeded that of previous, passive foil exposure experiments by more than an order of magnitude. Further analyses of these samples have been undertaken using the Field Emission Gun Scanning Electron Microscope (FEGSEM) facility in the University of Leicester's Advanced Microscopy Centre to provide much higher spatial resolution images of the impact features, revealing the detailed morphologies of impact perforations with diameters less than 100 nm. Energy Dispersive X-ray

Spectroscopy (EDXS) facilities at the Natural History Museum, London, and the Focussed Ion Beam Secondary Ion Mass Spectroscopy (FIBSIMS) facility at Imperial College, London, have also been used to search for post-impact residues on the films. The results of this work are inconclusive, primarily because of the trace quantities of material remaining in the rim of a hole post impact, and are not reported in detail here.

[8] In this paper are present images of the impact features, including nanometer-scale impact holes whose observed morphologies are used to infer incident directions for the impacting particles and their particle diameters and to discriminate different particle populations. The analyses show a high density of particles in the ISS environment, most of which are secondaries generated locally, following larger impacts elsewhere on the ISS, or are particles released during docking maneuvers by Progress supply spacecraft. In addition to these local populations the morphologies indicate the presence of previously undetected nanometer-scale dust particles which may not be local in origin and which have impacted at hypervelocity. Hypervelocity impacts are typical for dust particles and occur when the relative velocity of the impactor and target is sufficiently large that the strength of a material is small compared with the inertial stresses during the impact. The particles detected have diameters greater than $\sim$10 nm and masses greater than $\sim$10^{-18} g. The detected flux is compatible with the predicted Grün micrometeoroid flux [*Grün et al.*, 1985] at approximately 10^{-18} g and may represent the first measurement of particles in this size regime at 1 AU or from Earth orbit. Streams of equivalent mass dust particles from Jupiter and Saturn have been detected at high velocities $>$100 km s^{-1} in the outer solar system [*Grün et al.*, 2001].

[9] The detection of a nanometer dust population and its separation from local particle flux demonstrates the effectiveness of thin film MCPs as sensitive passive dust detectors. Building on the serendipitous findings of the initial exposure, we propose future possibilities for the technology in both (1) optimized passive sensors requiring retrieval and postexposure analysis and (2) as active detectors of nanometer-scale interplanetary and interstellar dust populations on nonretrievable platforms.

2. Imaging and Analysis Techniques

[10] SE imaging with a tungsten source SEM at the Advanced Microscopy Centre (AMC) at the University of Leicester was shown previously to have insufficient spatial resolution, when applied to these extremely thin Al films, to image holes smaller than $\sim$500 nm [*Carpenter et al.*, 2005]. The SEM's performance was limited by the requirement to operate the SEM with low electron beam currents, to prevent excessive charging of the thin film, and low accelerating voltages ($<$2 kV), to minimize the penetration depth of the electron beam in the film. SEM imaging was therefore only appropriate for resolving impact damage by particles whose ballistic limits (F_{max}), defined as the maximum thickness of aluminum which can be perforated by an impact [*McDonnell et al.*, 2001], were much greater than the film thickness f. An FEI Sirion 200, an ultrahigh-resolution Schottky Field Emission Scanning Electron
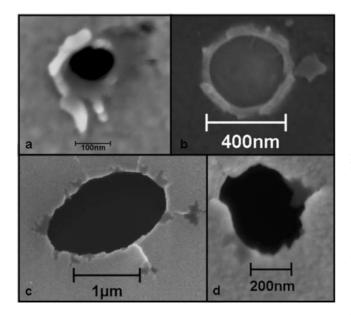
Figure 1. Secondary electron Field Emission Gun Scanning Electron Microscope (FEGSEM) images of holes in the Al film which are representative of the different morphologies observed. (a) Type 1: one of the smallest holes observed in the Al film with a diameter of 104 nm which is typical of an impact at hypervelocity. (b) An impact crater on the aluminum coated glass interchannel web. (c) Type 2: an elliptical hole in the film. The morphology is not typical for hypervelocity and may indicate a slow impact. (d) Type 3: an irregularly shaped hole in the film.

Microscope in the Advanced Microscopy Centre of the University of Leicester, has been used to provide new images the impact holes revealing structure in the morphology of holes on the scale of 100 nm. SE images were produced with the FEGSEM using an accelerating voltage of 2 kV. At very high magnifications the film was found to become charged very quickly; this effect may have been aggravated by the contamination of the films which occurred during exposure on the ISS [*Carpenter et al.*, 2006]. Charging of the film, manifested as a loss of focus followed by a brightening and loss of contrast in the SE images, was the limiting factor in the achievable image resolution and picture quality, which varied between holes.

[11] For each impact hole a value for the circularity c, defined as 4π (hole area/perimeter^2) was calculated. A c value of 1.0 indicates a perfect circle, while a value approaching zero indicates an increasingly elongated or freeform shape. The circularity value can be used as a filter to remove highly irregular hole shapes, resulting from tears in the film, from the analysis. The diameters of the holes were then determined, the diameter (D_h) being defined by the mean of the lengths of the major axis (L) and minor axis (D) of the best fit ellipse. Ellipses were fitted to the open areas of the holes, which appear black in SE images. This method provides a common and consistent measurement for hole shapes observed on the sample. This image analysis was carried out using the free image analysis software ImageJ (available at http://rsb.info.nih.gov/ij/).

[12] The major and minor axes of the best fit ellipse to a hole were also used to infer possible incident directions for the incident particles. For a perfectly spherical particle, with a diameter $d_p > 10f$, at grazing incidence on a thin foil the aspect ratio $L{:}D$ of the elliptical hole produced following an impact will be related to the incident angle ϕ, measured from the normal to the surface, by the relation $D/L = \cos \phi$ [*McDonnell and Gardner*, 1998]. This relationship cannot account for irregular morphologies which are believed to be produced by irregularly shaped particles which punch out their cross sections from the foils [*McDonnell and Gardner*, 1998]. The angle ϕ is referred to below as the angle of elevation from the surface of the film. The direction of the ellipse's major axis can also be used to infer two possible azimuthal angles θ for the particle in the plane of the film's surface. The angle of elevation ϕ and the azimuthal angle θ together define two possible incident directions for the impacting particle. By combining this information with knowledge of the sample pointing direction and orientation during exposure the particle incident directions with respect to the surrounding ISS structure can be deduced.

[13] From the measured values of D_h the diameters of particles (d_p) incident at hypervelocity can be determined, if the velocity and density of the particles are known, by applying empirical formulae generated from laboratory impact data [*Gardner et al.*, 1997; *Carey et al.*, 1985; *Sawle*, 1969; *Nysmith and Denardo*, 1969; *Maiden et al.*, 1963]. Of the available equations, only those of *Carey et al.* [1985] (the CMD formula) and *Gardner et al.* [1997] (the GMC formula) attempt to characterize hole growth for impacts where $D_h \sim f$. The GMC formula is scaled to experimental impact data from *Hörz et al.* [1994] and is generally more reliable close to the ballistic limit than the CMD formula. The GMC formula is therefore used here to calculate particle diameters. An uncertainty in the results arises because the GMC formula has been determined from laboratory impacts on much thicker foil targets. Extrapolating the GMC formula to the nanoscale regime and to thin evaporated films may be unjustified, but in the absence of more appropriate formulae it offers the best available approximation.

[14] Additional information on particle properties has been provided by visual inspection of the hole shapes. Figure 1 shows SE images of a number of different impact holes with differing morphologies and spatial scales representing the different types of impact hole observed in the aluminum film. Each image has a dark region in which all aluminum has been removed by the impact. This area is used to define a hole's area. Figure 1a shows a hole in the film with a measured diameter of 104 nm. This hole has a shape which may be considered typical of hypervelocity impact (HVI), i.e., a regular shape with a raised rim. Impact holes of this type are denoted here as having "type 1" morphology. This structure for hypervelocity impacts by dust particles on the nanometer scale is consistent with observations of craters (in which the foil is not perforated) of similar diameters observed in analysis of much thicker foils exposed to dust from comet Wild 2 on the Stardust mission [*Hörz et al.*, 2006]. Figure 1a is an example of one of the smallest holes imaged, which have diameters close to the thickness of the film f and are likely to have a HVI origin. These holes are close to the particle detection limit/
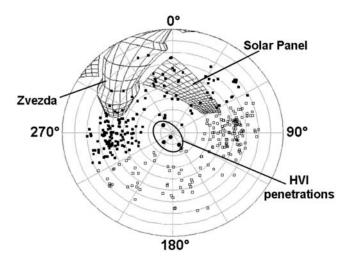
Figure 2. Incident directions of the impacting particles on the nanofilms shown over the hemispherical field of view of the samples from their location on the "Pirs" module of the International Space Station (ISS). The radial direction is elevation angle ϕ from 0° at the center to 90° at the edge of the hemispherical view. Azimuthal angles θ are shown on the image around the circumference of the plot. The solid and open squares indicate alternative possible incident directions for each particle. The circles are type 1, hypervelocity impact (HVI), penetrations indicative of dust particles and for which only one of the two possible incident directions is shown. The hemispherical view of the ISS from the samples is used courtesy of Boeing and was provided by C. Soares (2005). The Zvezda module is visible on the left and lies along the ISS's negative x axis.

ballistic limit F_{max}, of the films as defined by *McDonnell and Sullivan* [1992] where $D_h = f$. The ballistic limit can also be defined at $D_h = 0$ [*Gardner et al.*, 1997], and holes have been observed in the film with diameters as small as $D_h = 0.4f$.

[15] The high-resolution FEGSEM imaging has also allowed the observation of a few craters in the aluminum-coated interchannel web, which were unobservable in earlier SEM images. An example is shown in Figure 1b. Identifying and imaging craters proved challenging, but those craters imaged successfully showed morphologies typical of HVI, although their properties are complicated by the aluminum-glass double layered structure of the target.

[16] Impact holes which are much larger than the film thickness vary in shape. Some, like that shown in Figure 1c, are elliptical but with irregular edges and do not have raised rims. Some also show cracking in the surrounding film. These elliptical holes are denoted here as holes with a "type 2" hole morphology. Irregularly shaped dark features visible in the images around some impact holes (of all sizes) may indicate subsurface damage to the films caused during the impact. Some of the largest holes ($D_h > 1$ μm) are associated with tears in the film. Other impact holes are more irregular in shape, like that in Figure 1d. These holes may be generated by particles with diameters much greater than the film thickness and may serve as a record of the

particle's shape [*McDonnell and Gardner*, 1998]. Alternatively, they may be the result of damage to the impact site post impact. Holes exhibiting this type are denoted here as having "type 3" morphology. The lack of a clearly raised rim for either type 2 or type 3 holes may indicate that they have been generated by slower particles. At very small diameters, holes without rims appear alongside those with rims, suggesting distinct populations of both HVI and slow particles. The irregular shapes and cracking of the film around the holes resemble larger-scale impact holes observed in retrieved multilayer insulation foils from the EURECA spacecraft [*Wright et al.*, 1995]. This may indicate a similar production mechanism.

3. Particle Incident Directions

[17] A total of 173 holes were imaged, and the angles θ and ϕ were determined for each one. The angles of incidence are displayed in Figure 2 on a hemispherical view of the ISS as seen from the sample. The ISS's Zvezda module and a solar panel are visible within the sample's field of view. Each hole has two possible inferred directions. Both are indicated in Figure 2, one with a solid square and one with an open square. The error in the determined direction for a particle is not known. In one configuration (solid squares) the impact directions may be closely aligned with the ISS structure (particularly the Zvezda module's portside solar panel) and the direction of the of the ISS's negative x axis. The x axis of the ISS is defined along the long axis of the Zvezda module, becoming more negative with increased distance from the samples and reaching its limit at the end of the Zvezda module. Aluminum surfaces from the Shuttle Plume Impingement Flight Experiment (SPIFEX) show impact craters produced by high-speed propellant droplet impacts with d_p values ranging from 1 to 20 μm [*Soares et al.*, 2002]. Such a mechanism may also be the source of some of the holes observed in the filmed MCPs. Particles originating from the negative x direction may have been released during thruster firings by Progress during docking maneuvers with Zvezda. Particles from the direction of the solar panel are likely to be secondaries following larger impacts as are particles originating elsewhere on the ISS structure.

[18] It is also possible that the directionality observed may have some natural origin. The negative ISS x axis will also be close to the mean solar direction observed by the particles over the 2 year exposure in an x axis perpendicular to orbital plane attitude. It may be that β meteoroids, meteoroids accelerated on hyperbolic orbits out of the solar system by radiation pressure [*Whipple*, 1976; *Wehry and Mann*, 1999], constitute this population or contribute to it. Alternatively, the directionality may indicate the presence of streams of nanometer-scale dust particles in near-Earth space, with trajectories dictated by the Earth's electric and magnetic fields, as has been observed at Jupiter and Saturn where the increased field strengths accelerate particles to velocities >100 km s^{-1}, thus making their detection possible with conventional dust detectors. In this scenario the incident directions not related to the ISS structure and indicated in Figure 2 as open squares are also possible. The most likely scenario, however, is that the majority of impact

holes, which have type 3 or type 4 morphologies, are due to particles generated locally.

[19]　It remains possible that the much rarer type 1 holes, of which four have been positively identified and which are much smaller and have been generated at much greater velocities, are due to a nonlocal population. The determined incident directions of the type 1 impactors are indicted in Figure 2. Only one of the two possible incident directions is shown for these particles. All impacts of this type are located close to the normal to the surface of the samples, the result of near-circular morphologies. This may indicate an alignment with this incident direction, but it is more likely that no direction can be inferred for these particles. HVI holes with diameters less than 10 times the target thickness will be approximately circular and do not provide a measure of particle incident direction by this technique [*Gardner et al.*, 1997].

4.　Particle Diameters, Mass, and Flux

[20]　The cumulative flux of holes in the film imaged using the FEGSEM was calculated to be 35 m^{-2} s^{-1}. This value was obtained by dividing the value of 173 holes imaged in the 0.12 mm^2 of area surveyed, multiplying by the 0.63 open area fraction of the MCPs, and dividing by the 6.5×10^7 s exposure time. The open area fraction of the film is the fraction of the total surface area which is free standing over the circular 12.5 μm channels. The area of the films surveyed was restricted by the small scale of images, the challenges in imaging at high resolution, and the facility time available for the survey.

[21]　Figure 3 shows the size distribution of holes in the exposed film with a circularity $c > 0.5$. This distribution follows an analysis of both SEM and FEGSEM images. A c value of 0.5 was selected because it was found through inspection that this circularity could be used to select hole shapes of interest. The number of holes observed within each diameter bin was divided by the area surveyed and the exposure time to give the particle flux within a given diameter bin. The value for particle flux for each diameter bin was then divided by the bin diameter to obtain the particle flux per micrometer of hole diameter. The flux is calculated by assuming a constant particle impact rate throughout the exposure. If the observed holes are the result of a single event, such as secondaries resulting from a larger impact elsewhere on the ISS or particles ejected during docking procedures by the Progress module, then the calculated flux values are no longer valid but the hole size distribution remains so.

[22]　Also shown in Figure 3 is the particle flux for holes with type 1 morphology, typical of HVI. The range of sizes of these holes is 40−250 nm. The uncertainty in the flux arises because of the statistical error in the small sample of four holes of this type which could be identified with certainty and the possible addition of five holes of similar size for which image quality was sufficiently poor because of charging effects that their identification as type 1 in origin was deemed uncertain. These type 1 holes represent a population that may be separated from those which have produced the other holes observed in the sample, are from a narrow range of incident directions, and are probably slower than hypervelocity and local to the ISS. These hypervelocity
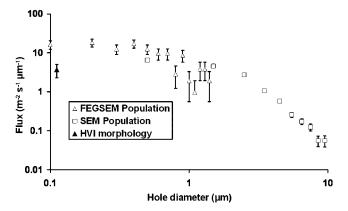

Figure 3. Flux as a function of hole diameter D_h determined from secondary electron images of impact features generated with the SEM and FEGSEM instruments and with a circularity >0.5. Errors in the data are statistical. Also shown are the flux of holes for which a typical HVI morphology was identified.

particles are likely to originate from a natural dust population or a debris population probably not local to the ISS.

[23]　The diameters of the particles which produced the holes were calculated using the GMC formula for which the velocity and density of the particles were required. A particle density of 2 g cm^{-3} is assumed here. The density of particles in the near-Earth dust population is typically 2.0−2.4 g [*McDonnell and Gardner*, 1998]. In the absence of any velocity information specific to the incident particles a particle velocity distribution for the known micrometeoroid and debris population, greater than 1 μm in diameter, was calculated using the European Space Agency's Meteoroid and Space Debris Terrestrial Environment Reference Model (MASTER) [*Oswald et al.*, 2005]. MASTER provides predictions of fluxes of impactors on spacecraft in different orbits as a function of particle type, mass, trajectory, and velocity based on measurements of impacts on returned spacecraft surfaces, ground-based observations, and theoretical models of the natural meteoroid background and debris populations. The smallest particles which can be modeled by MASTER are 1 μm in diameter. The most recent version of this model, MASTER 2005 [*Oswald et al.*, 2005], has been used here to model the micrometeoroid and debris fluxes on a flat plate on the ISS representative of the returned MCP samples. The ISS orbit is modeled with a semimajor axis of 6725.65 km, an eccentricity of 9×10^{-4}, an inclination of 51.6°, a right ascension of ascending node of 199.76°, and an argument of perigee of 274.3°. The pointing direction of the samples during the exposure was 49.5° to the right of the negative x axis in the standard ISS coordinate system. The negative x axis corresponds to the space station's wake direction for a standard local vertical, local horizontal (LVLH) attitude, and so under these conditions the point (0,0) in Figure 2 is in a direction 49.5° to the right of wake. Although the intended attitude for the ISS is LVLH, during construction the ISS attitude is varied between LVLH and an attitude in which the x axis is perpendicular to the orbital plane. Because the ISS attitude is variable, the pointing direction of the samples over the
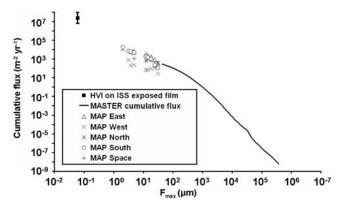
Figure 4. Cumulative flux of holes in aluminum foils of varying thicknesses (ballistic limits) F_{max} for surfaces in an ISS orbit and with equivalent pointing direction to that of the microchannel plate (MCP) films during the exposure as predicted by the Meteoroid and Space Debris Terrestrial Environment Reference Model (MASTER) 2005 model of space debris and natural meteoroid fluxes. Also shown are cumulative fluxes for foils exposed as part of the Multiple-Foil Microabrasion Package (MAP) experiment on the Long Duration Exposure Facility (LDEF). The cumulative flux of particles measured on the MCP nanofilm is also shown.

period of the exposure is assumed to be equivalent to that of a randomly tumbling surface. The mean impact velocity for the particles, accounting for the motion of the ISS, is calculated to be 18.5 km/s.

[24] For each particle in the Monte Carlo simulation described above, MASTER 2005 was used, with the ballistic limit formula of *McDonnell and Sullivan* [1992], to determine F_{max}. The calculated cumulative number of holes as a function of foil thickness is shown in Figure 4 for the MCP sample's exposure history for $F_{max} > 45$ μm. For smaller sizes, MASTER undersamples the particle population because of lower limits imposed on the particle diameters for the various populations. Figure 4 also shows flux versus F_{max} data from the Multiple-Foil Microabrasion Package (MAP) experiment on LDEF. The directions given for MAP foils in Figure 4 are the pointing directions in an Earth-based reference frame, where "space" is the zenith direction. The values presented are taken from *McDonnell and Stevenson* [1991]. Also shown is the cumulative flux of particles observed in the 60 nm film for which a type 1 HVI impact morphology was identified. In this case only holes with diameters $D_h > f$ are considered because this is where F_{max} is defined by the ballistic limit equation used with MASTER 2005. The errors shown in Figure 4 indicate the maximum and minimum possible particle flux possible within a 95% certainty according to the statistical method described by *Grün et al.* [2001]. Figure 4 illustrates the increase in sensitivity offered by the foils compared with previous foil exposure experiments but also shows that the detected flux is somewhat large compared with a continuation of the known flux versus F_{max} distribution, which rolls off for ballistic limits below approximately 100 μm. The flux of dust and debris particles with small diameters is observed to roll off in this size regime and is a property of

the natural interplanetary dust environment which at smaller sizes, still inverts and increases again.

[25] The inversion of the roll off in flux toward very small particle sizes is described by the "Grün flux" [*Grün et al.*, 1985] of interplanetary dust particles, which is generally used to quantify the natural sporadic meteoroid flux at 1 AU. It is expressed as the cumulative flux of particles with masses above a given value which are incident on a randomly tumbling plate. The distribution does not account for the increase in flux at Earth due to gravitational focusing, which at 400 km, is by a factor 1.99 [*McDonnell et al.*, 2001], or for occultation of the tumbling plate's field of view by the Earth, which at 400 km, is a factor 0.63 [*McDonnell et al.*, 2001]. The Grün flux applies to particles with masses greater than 10^{-18} g. The increase in flux for particles with masses lower than $\sim 10^{-11}$ g is due to the presence of the so-called β meteoroids, small particles for which the ratio β of the force due to solar radiation pressure and gravity is greater than 1. These particles, first identified by *Berg and Grün* [1973], are accelerated on hyperbolic orbits out of the solar system because of the effects of radiation pressure and the Lorenz force and are incident from within a few degrees of the solar direction. A significant property of the β meteoroids is a velocity $v > 40$ km s^{-1}, much greater than that of the general meteoroid population. An accepted lower mass limit for β meteoroids is $\sim 5 \times 10^{-16}$ g [*Wehry and Mann*, 1999].

[26] For the smallest particles the Lorenz force will dominate dynamics as β falls off and the charge to mass ratio becomes large. These particles will experience acceleration due to interplanetary electromagnetic forces close to the Sun, in interplanetary space, and in the environment near Earth. A detailed description of the dynamics of charged dust particles in the solar system is given by *Horanyi* [1996]. Figure 5 shows the Grün flux for particles with diameters greater than 10^{-18} g. Also shown in Figure 5 is the single cumulative flux data point established for HVI particles on the exposed, filmed MCPs. For each hole
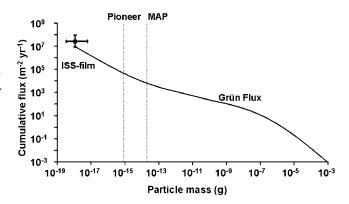

Figure 5. Cumulative flux as a function of particle mass given by the Grün model for the flux of interplanetary dust particles at 1 AU. Also shown is the cumulative flux of hypervelocity impacts on the 60 nm film below the threshold mass for detection by the film. Also shown by dotted lines are approximate values of the minimum particle masses which could perforate the $f = 2$ μm MAP foils at 40 km s^{-1} and which were detected from the solar direction by the dust detectors on Pioneer 8 and 9.

identified to have a HVI origin a particle diameter was calculated using the GMC equation assuming a 40 km s^{-1} velocity. The possible range of particle sizes detected was calculated to be 12–37 nm, giving a mass range of 1.8×10^{-18} to 5.1×10^{-17} g. Although the sample of images was insufficiently large to generate a particle size distribution, it is sufficient to calculate an upper and lower limit for the cumulative flux of particles with a diameter greater than that at the ballistic limit of the film, which at 40 km s^{-1}, is calculated, using the GMC formula at the limit $D_h = 0$, to be 1.5×10^{-18} g for a particle density of 2.0 g cm^{-3}. The measured flux shown in Figure 5 is 2.4×10^7 particles m^{-2} yr^{-1}, after adjustment to remove the effects of gravitational enhancement, occultation by the Earth, and occultation of the experiment's field of view by the spacecraft structure shown in Figure 2 (a factor of 0.73). The error in particle mass, shown in Figure 2, results from the uncertainty in the particle velocities. The velocities used to calculate the uncertainty in mass range between 18.5 km s^{-1} (the mean relative velocity calculated for the micrometeoroid and debris populations modeled using MASTER 2005), to give a mass upper limit, and 70 km s^{-1} (the maximum velocity for micrometeoroids), to give a mass lower limit. The data point intersects the micrometeoroid flux predicted in this size regime, which has never before been examined experimentally by dust particle detectors, either passive or active, although β meteoroids with masses $>10^{-15}$ g have been detected by dust detectors on missions including Pioneer 8 and 9, HEOS, and Ulysses spacecraft. It remains possible, however, that the flux observed here is due to or is contaminated by a flux of nanometer-scale debris particles in low Earth orbit, in which case this represents a previously unexamined population of debris particles.

5. Summary and Conclusions

[27] Microchannel plates bearing thin aluminum films over their faces have been exposed on the outside of the International Space Station and examined in the laboratory postretrieval using a combination of SEM and FEGSEM imaging techniques. Holes have been observed in the films, which have been generated by small impacting particles. The smallest of these holes are just a few tens of nanometers in diameter, and thus the smallest particles incident on the films must have been smaller than the diameter of these holes.

[28] Several different impact morphologies have been identified in the high-magnification SE images generated using a FEGSEM. The impact morphologies have been related to various properties of the impacting particles. Some of the smallest holes observed, with diameters similar to the film thickness, have morphologies typical of larger-scale hypervelocity impact holes in microscopic foils showing a high degree of circularity and regularity and having raised rims around their edges. Some smaller holes and those with diameters much larger than the film thickness have morphologies which are less typical of HVI processes, lacking raised rims, smooth edges, and highly circular shape. Features of this kind are the dominant impact features on the samples. The variation of morphology from that typical of HVI may be related to the properties of the

films which differ from those with typical microscopic and macroscopic impact target thicknesses; however, the presence of impact features which are typical of HVI at smaller sizes indicates that this may not be the case, and it is most likely these holes are generated by slow particles. Slow particles detected by the samples are likely to have originated locally to the samples on the ISS, whereas particles incident at hypervelocity are more likely to be representative of a general dust or debris population in low Earth orbit. No experimental data on the effects of hypervelocity impacts on thin films or impacts by nanometer-scale dust particles currently exist in the literature, and it is possible that the effects of impacts by very small particles on nanometer-scale evaporated films vary from those on larger-scale foils. There is a resultant uncertainty in any impactor properties inferred from impact morphologies. An investigation is underway at the University of Leicester into impacts by nanometer-scale dust particles on thin films, the findings of which will be reported in a future paper. An interpretation of particle properties and discrimination between hypervelocity and slow impacts based on hole morphology can be carried out with increased certainty when experimental verification of nanometer impact effects is available.

[29] An analysis of the angles of incidence of the particles based on the shapes of impact holes indicates that the majority of holes can be related to specific incident directions. These directions may be related to the ISS structure and indicate that the particles whose impacts generated the holes analyzed were secondaries, following larger impacts elsewhere on the ISS, or are related to docking maneuvers by the Progress supply spacecraft. Alternatively, there is a possibility that the directionality of the particles is a natural phenomenon, but this seems unlikely given that the morphologies of the holes which have been used to infer directionality are not typical of HVI and the fluxes measured for holes with diameters greater than 0.5 μm are much larger than values detected by previous experiments in low Earth orbit, which have been sensitive to particles of this size regime. Very small holes with HVI morphology cannot be used to infer incident directions with a simple cosine dependence.

[30] An application of the GMC equation to determine particle diameters for holes resulting from HVI reveals that particles as small as 10 nm and with masses as small as or less than 10^{-18} g may have been detected. These are the smallest dust particles ever detected in near-Earth space and represent a 2 order of magnitude increase to the minimum mass of detectable dust populations detected by previous in situ experiments. In addition, the flux detected for particles of this size intersects the predicted "Grün flux" of micrometeoroids of this size at 1 AU, within the significant statistical errors. In the size regime $m < 10^{-10}$ g, fluxes are primarily due to β meteoroids whose dynamics are dominated by radiation pressure. These particles become injected into hyperbolic orbits on which they are accelerated out of the solar system. For particles with masses as low as 10^{-18} g the role of the Lorenz force becomes increasingly important, and their orbital histories may differ significantly from those of larger particles. The detection of particles with very low masses may therefore provide access to new parent bodies, processes in the solar system, and interstellar dust particles.

[31] The origins of the nanometer particles observed during this exposure of the ISS cannot be identified with certainty, and either a debris or interplanetary dust origin is possible. However, the results reported here highlight the possibility that a population of nanometer-scale dust particles exists in near-Earth space. Regardless of the origins of the particles observed, the observation technique described offers access to populations in a new size-velocity regime which could not be accessed by previous passive experiments like the 2 μm thick foils on the MAP passive foil experiment. The most sensitive measurements made to date of the β meteoroids have been made by the active sensors on the Pioneer 8 and 9 spacecraft, which were sensitive to masses as low as 10^{-13} g at 20 km s^{-1}. The minimum particle mass which can be detected by the thin films at 20 km s^{-1} is 6.7×10^{-18} g. The exposure of the films was not optimized for the detection of dust particles, and the survey carried out on the samples to date has been limited, leading to large uncertainties in the data presented. There is a need for optimized exposures and more extensive surveying of the samples to reduce the uncertainties in the origin and magnitudes of the measured particle flux.

[32] We look forward to future optimized experiments on the ISS and other platforms in which passive nanofilm detectors will be used to investigate the nanometer dust population through postretrieval laboratory analysis. For future exposures the location for experiments on platforms such as the ISS should be optimized for dust detection. A major source of uncertainty in the described analysis is particles related to the ISS structure and spacecraft docking procedures. Future experiments should have fields of view with minimal obscuration by spacecraft structure and should minimize the fraction of the field of view which contains space likely to be used during docking procedures and maneuvers. Although removing structure from line of sight does not remove the risk of contamination, the extent of cratering, and penetration by secondary and other local particles is minimized. In the future, a more extensive high-resolution survey of the previously exposed thin film samples will be performed in order to increase the sample of hypervelocity impact features imaged and allow a flux versus particle size distribution for the dust particles to be produced. Such a distribution can be compared with existing models and data sets to identify the origin of the particle population and provide a continuation to the existing experimental flux versus particle properties data set.

[33] Work is ongoing to investigate impact processes on the thin films and also to extend the passive sensor concept by the addition of an active readout mechanism. An active dust detector based on the thin film concept would be sensitive to nanometer-scale dust particles and would be suitable for flight on nonretrievable platforms and beyond low Earth orbit.

References

Auer, S. (2001), Instrumentation, in *Interplanetary Dust*, edited by E. Grün, pp. 385–444, Springer, London.

Berg, O. E., and E. Grün (1973), Evidence of hyperbolic cosmic dust particles, *Space Res.*, *13*, 1046–1055.

Carey, W. C., J. A. M. McDonnell, and D. G. Dixon (1985), Capture cells: Decoding the impacting projectile parameters, *Lunar Planet. Sci.*, *XVI*, 111–112.

Carpenter, J. D., T. J. Stevenson, G. W. Fraser, J. S. Lapington, and D. Brandt (2005), Dust detection in the ISS environment using filmed microchannel plates, *J. Geophys. Res.*, *110*, E05013, doi:10.1029/2004JE002392.

Carpenter, J. D., T. J. Stevenson, and G. W. Fraser (2006), Damage and contamination to filmed microchannel plates on the International Space Station, *J. Spacecr. Rockets*, *43*(1), 194–199.

Divine, N. (1993), Five populations of interplanetary meteoroids, *J. Geophys. Res.*, *98*, 17,029–17,048.

Drolshagen, G., et al. (1996), Optical survey of micrometeoroid and space debris impact features on EuRECA, *Planet. Space Sci.*, *44*, 317–340.

Fraser, G. W., et al. (2001), LOBSTER-ISS: An imaging X-ray all-sky monitor for the International Space Station, *Proc. SPIE Int. Soc. Opt. Eng.*, *4497*, 115–126.

Gardner, D. J., J. A. M. McDonnell, and I. Collier (1997), Hole growth characterisation for hypervelocity impacts in thin targets, *Int. J. Impact Eng.*, *19*(7), 589–602.

Grün, E., H. A. Zook, H. Fechtig, and R. H. Giese (1985), Collisional balance of the meteoritic complex, *Icarus*, *62*, 244–272.

Grün, E., M. Baguhl, H. Svedhem, and H. A. Zook (2001), In situ measurements of cosmic dust, in *Interplanetary Dust*, edited by E. Grün, pp. 295–346, Springer, London.

Hofer, S. (2004), X-ray mirror expose experiment on ISS, *Rep. Expose-KT-RP-001*, Kayser-Threde GmbH, Munich, Germany.

Horanyi, M. (1996), Charged dust dynamics in the solar system, *Annu. Rev. Astron. Astrophys.*, *34*, 383–418.

Hörz, E., M. Cintala, R. P. Bernhard, and T. H. See (1994), Dimensionally scaled penetration experiments: Aluminum targets and glass projectiles 50 μm to 3.2 mm in diameter, *Int. J. Impact Eng.*, *15*(3), 257–280.

Hörz, F., et al. (2006), Impact features on Stardust: Implications for comet 81P/Wild 2 dust, *Science*, *314*, 1716–1719.

Maiden, C. J., J. W. Gehring, and A. R. McMillan (1963), Investigation of fundamental mechanism of damage to thin targets by hypervelocity projectiles, *Rep. TR63-225*, GM Defense Res. Lab., Santa Barbara, Calif.

McDonnell, J. A. M., and D. J. Gardner (1998), Meteoroid morphology and densities: Decoding satellite impact data, *Icarus*, *133*, 25–35.

McDonnell, J. A. M., and T. J. Stevenson (1991), Hypervelocity impact microfoil perforations in the LEO space environment (LDEF, MAP AO 023 experiment), in *LDEF, 69 Months in Space: First Post-Retrieval Symposium*, edited by A. S. Levine, pp. 443–458, NASA, Washington, D. C.

McDonnell, J. A. M., and K. Sullivan (1992), Hypervelocity impacts on space detectors: Decoding the projectile parameters, in *Hypervelocity Impacts in Space*, edited by J. A. M. McDonnell, pp. 39–47, Univ. of Kent at Canterbury, Canterbury, U. K.

McDonnell, J. A. M., S. P. Deshpande, D. H. Niblett, M. J. Neish, and P. J. Newman (1993), Near Earth space impact environment—An LDEF overview, *Adv. Space Res.*, *13*(8), 87–108.

McDonnell, J. A. M., N. McBride, S. F. Green, P. R. Ratcliff, D. Gardner, and A. D. Griffiths (2001), Near Earth environment, in *Interplanetary Dust*, edited by E. Grün, pp. 163–261, Springer, London.

Nysmith, C. R., and B. P. Denardo (1969), Experimental investigation of the momentum transfer associated with impact into thin aluminum targets, *NASA Tech. Note, TND-5492.*

Oswald, M., P. Wegener, S. Stabroth, C. Wiedemann, J. Rosebrock, C. Martin, H. Klinkrad, and P. Vörsmann (2005), The MASTER 2005 model, in *Proceedings of the 4th European Conference on Space Debris*, edited by D. Danesy, pp. 235–243, Eur. Space Agency, Darmstadt, Germany.

Sawle, D. R. (1969), Hypervelocity impact in thin sheets and semi-infinite targets at 15 km/s, *AIAA J.*, *8*(7), 1240–1244.

Soares, C., H. Barsamian, and S. Rauer (2002), Thruster plume induced contamination measurements from the PIC and SPIFEX flight experiments, *Proc. SPIE Int. Soc. Opt. Eng.*, *4774*, 199–209.

Srama, R., and E. Grün (1997), The dust sensor for CASSINI, *Adv. Space Res.*, *20*(8), 1467–1470.

Srama, R., S. Kempf, G. Moragas-Klostermeyer, M. Langraf, S. Helfert, Z. Sternofsky, M. Rachev, and E. Grün (2007), Laboratory test of the

large area mass analyser, in *Dust in Planetary Systems*, *Eur. Space Agency Spec. Publ.*, *ESA SP-643*, 209–212.

Wehry, A., and I. Mann (1999), Identification of beta-meteoroids from measurements of the dust detector onboard the Ulysses spacecraft, *Astron. Astrophys.*, *341*, 296–303.

Whipple, F. L. (1967), On maintaining the meteoritic complex, in *The Zodiacal Light and the Interplanetary Medium*, edited by J. L. Weinberg, pp. 409–462, U.S. Gov. Print. Off., Washington, D. C.

Whipple, F. L. (1976), Sources of interplanetary dust, in *Interplanetary Dust and Zodiacal Light; Proceedings of the Colloquium, 31st, Heidelberg, West Germany, June 10–13, 1975*, pp. 403–415, Springer-Verlag, Berlin.

Wright, I. P., A. Sexton, and M. M. Grady (1995), EURECA multi-layer insulation impact morphology and residue analysis, final report, contract RFQ/3-8001/94/NL/JG, Eur. Space Agency, Paris.

————————————

J. C. Bridges, J. D. Carpenter, G. W. Fraser, and T. J. Stevenson, Space Research Centre, Department of Physics and Astronomy, Michael Atiyah Building, University of Leicester, University Road, Leicester LE1 7RH, UK. (jdc13@star.le.ac.uk)

R. J. Chater, Department of Materials, Imperial College London, Exhibition Road, London SW7 2AZ, UK. (r.chater@imperial.ac.uk)

S. V. Hainsworth, Department of Engineering, University of Leicester, University Road, Leicester LE1 7RH, UK. (svh2@leicester.ac.uk)

A. T. Kearsley, Natural History Museum, Cromwell Road, London SW7 5BD, UK. (antk@nhm.ac.uk)